remote sensing

MDPI

Article

Mapping Annual Land Disturbance and Reclamation in a Surface Coal Mining Region Using Google Earth Engine and the LandTrendr Algorithm: A Case Study of the Shengli Coalfield in Inner Mongolia, China

Wu Xiao [1,2], Xinyu Deng [1], Tingting He [2,*] and Wenqi Chen [1]

[1] Department of Land Management, Zhejiang University, Hangzhou 310058, China; xiaowu@zju.edu.cn (W.X.); xinyudeng@zju.edu.cn (X.D.); 21922079@zju.edu.cn (W.C.)

[2] Institute of Land Reclamation and Ecological Restoration, China University of Mining and Technology, Beijing 100083, China

* Correspondence: tthe2011@student.cumtb.edu.cn

Received: 3 April 2020; Accepted: 15 May 2020; Published: 18 May 2020

Abstract: The development and utilization of mining resources are basic requirements for social and economic development. Both open-pit mining and underground mining have impacts on land, ecology, and the environment. Of these, open-pit mining is considered to have the greatest impact due to the drastic changes wrought on the original landform and the disturbance to vegetation. As awareness of environmental protection has grown, land reclamation has been included in the mining process. In this study, we used the Shengli Coalfield in the eastern steppe region of Inner Mongolia to demonstrate a mining and reclamation monitoring process. We combined the Google Earth Engine platform with time series Landsat images and the LandTrendr algorithm to identify and monitor mining disturbances to grassland and land reclamation in open-pit mining areas of the coalfield between 2003 and 2019. Pixel-based trajectories were used to reconstruct the temporal evolution of vegetation, and sequential Landsat archive data were used to achieve accurate measures of disturbances to vegetation. The results show that: (1) the proposed method can be used to determine the years in which vegetation disturbance and recovery occurred with accuracies of 86.53% and 78.57%, respectively; (2) mining in the Shengli mining area resulted in the conversion of 89.98 km^2 of land from grassland, water, etc., to barren earth, and only 23.54 km^2 was reclaimed, for a reclamation rate of 26.16%; and (3) the method proposed in this paper can achieve fast, efficient identification of surface mining land disturbances and reclamation, and has the potential to be applied to other similar areas.

Keywords: surface mining; land disturbance trajectory; Google Earth Engine; LandTrendr algorithm; Landsat data

1. Introduction

Rapid economic and social development have driven increasing demand for mineral resources. However, as mining activities occupy and also damage land resources, the exploitation of these resources often has a significant impact on the ecological environment [1], leading to various secondary environmental problems such as land loss, land occupation, vegetation degradation, and soil erosion [2]. Therefore, mining and urbanization are currently regarded as the economic activities that have the most destructive impacts on natural ecosystems. These activities have various negative environmental consequences, and the governments of many countries require that areas degraded by mining be recovered. Open-pit mining, ore mining, and placement of soil cover (overburden dumps) following

strip mining can cause changes in land cover and land use. Land-cover changes around large surface mines have already caused serious environmental landscape degradation in parts of the USA [3]. Sustainable mining and green mining both require continuous monitoring of these changes to identify the long-term impacts on the environment and land cover. Monitoring such changes can then provide basic security measures as well as basic data for use in formulating land reclamation and ecological restoration strategies. In addition, quantifying the spatiotemporal changes in an area as a result of surface mining is particularly important for understanding the effects of mining activities and for assessing their ecological, environmental, and socioeconomic impacts [4].

Disturbances to land and vegetation caused by open-pit mining are key concerns for researchers and land management agencies. There have been numerous studies of the changes caused by mining at the micro-level, including changes to the physical and chemical properties of land [5], vegetation disturbance [6], and ground subsidence [7]. Before the advent of widespread remote-sensing techniques, field investigation had been an effective means of obtaining information about ground-level damage and surface monitoring prior to reclamation. However, due to the historical legacy of past mining, field surveys and studies cannot determine quantitative changes, and are rather slow and expensive.

Advances in satellite-to-ground observation technology have made remote sensing an effective method of measuring the nature and extent of vegetation [8]. The earliest application of remote-sensing data was in comparisons between data for different years. Satellite remote-sensing detection can be performed visually or by using computer-aided interpretation via automatic pattern recognition technology [9,10]. Remote-sensing technology can monitor and evaluate vulnerable landscapes, natural resources, ecosystems, and biodiversity conservation areas cost-effectively. In recent decades, extensive studies have been conducted on the use of low- and medium-resolution optical satellite data, including Landsat and MODerate-resolution Imaging Spectroradiometer (MODIS), to monitor the impacts of mining activities on ecosystems [11–13]. In addition, radar satellite data have been used to observe the deformations resulting from surface subsidence in mining areas [14].

The methods for monitoring mining disturbance and reclamation activities include various remote sensing classification methods. Several studies have measured coal mining surface disturbance using vegetation indices, such as the Normalized Difference Vegetation Index (NDVI), the Enhanced Vegetation Index (EVI), etc., which can typically be applied to monitoring via remote sensing. For example, a time series NDVI has been used to monitor mining-related grassland vegetation disturbances [15,16]. Jia et al. [17] and Li et al. [18] both studied the land damage and restoration processes associated with grassland open-pit and rare-earth mining using the Single Spectrum Analysis (SSA)-Mann Kendall and CART classification on multi-source time series NDVI, respectively. Multivariate change detection has been used to measure the expansion and spread of gold mining on the ground during two time periods [19]. Machine learning algorithms such as support vector machines and random forests have also been used to study land use classification in mining areas [20].

Monitoring studies have evolved from the use of several images to yearly time series of images. More recent studies have focused on using data with various levels of resolution to analyze and identify the spatiotemporal process of vegetation disturbance [21] and evaluate the effects of land reclamation [22,23]. This type of research is currently focused on monitoring the changes in time series remote-sensing data. For example, Townsend et al. [24] used the Landsat time series between 1976 and 2006 to detect changes in Central Appalachian surface mining and reclamation areas. Time series remote-sensing data can also be used to analyze the impact of surface mining on cultivated land and food security [25]. However, this method of manual interpretation and classification using multi-period images produces a heavy workload and readily accumulates classification errors.

Another problem is that the yearly image from a particular time node in a specific year can often only represent the vegetation and land use on the surface in a transient state. It cannot recognize characteristics that might change over a period of time. This makes monitoring events with nonlinear or highly spatiotemporal heterogeneity difficult. Often, annual data are available only for different time points in each year due to factors such as satellite transit time and weather conditions, including

cloud cover [26]. In many studies in which satellite images for the vegetation growth period have been selected, these data are usually for a specific time period between May and September [27]. This, however, challenges the credibility and comparability of the monitoring results.

In recent years, the development of cloud computing technology has made possible the use of available, massive remote-sensing satellite transit data for detecting changes in fine-grained, high-temporal-resolution data. The Google Earth Engine (GEE) launched by the American multinational technology company Google LLC has collected common remote-sensing data sets such as MODIS, Landsat, and Sentinel [28], and can use online or offline programming to obtain and process shared data. Cloud computing analyzes and processes remote-sensing data, thereby avoiding the tedious processes of data downloading and preprocessing required by traditional remote-sensing analysis models. The GEE platform offers strong data analysis and processing capabilities, and is gradually being applied to areas such as urban expansion [29], dynamic monitoring of ecological quality [30,31], and the monitoring of vegetation coverage [32].

Related algorithm-based technologies for time series remote-sensing change monitoring have also led to rapid progress, and the use of time series remote-sensing data analysis has increased in recent years. Current vegetation disturbance detection methods are now quite mature, with many excellent algorithms [33]. They are used to monitor changes in land cover by analyzing images as temporal sequences. These time series algorithms have enabled time series fitting based on the spectral index of vegetation, using methods such as the best index slope extraction (BISE) algorithm, time series decomposition methods such as wavelet changes, breakpoint detection algorithms based on time series segmentation such as the vegetation change tracker (VCT) model [34] and the LandTrendr algorithms [35], and multiclass times series curve detection algorithms such as the continuous change detection and classification (CCDC) [36].

Based on the premise that vegetation index patterns change over time along particular trajectories, mines can be differentiated from undisturbed natural areas because the trajectories of reclaimed mines differentiate them from urban disturbances [37]. Long-term sequence change detection methods are classified into four main types: spectral variables, image classification, spectral trajectory-based analysis, and data fusion methods [38]. The currently popular Landsat-based time series algorithms come mainly from North America. These include the Landsat interference and trend monitoring algorithm LandTrendr (for Landsat-based detection of trends in disturbance and recovery), which uses spectral trajectories developed by Oregon State University and the United States Forest Service, first proposed by Kennedy et al. [35]. It is used primarily in forest change detection, but has gradually been extended to areas of water and to cities. There are also other fields of application, such as the use of water probability to generate surface water change maps [39]. The advantages of LandTrendr are that it relies on Landsat archive data that can be accessed for free, and it is simple to operate. It can provide useful data for environmental assessment and remediation, including raster maps of bands that represent change trends, identification of points in time when abrupt changes occur, and analysis of various changing pixel attributes to promote better environmental assessment. The LandTrendr algorithm has been used to detect and analyze the timing of damage caused by surface mining [40].

In this study, in order to identify the spatiotemporal processes of surface mining and land reclamation more efficiently and accurately, an attempt was made to synthesize year-round images for the study period and the study area using the GEE cloud computing platform and the LandTrendr algorithm. The process can be summarized as data preprocessing, NDVI extraction, LandTrendr processing of the yearly trajectories, and mapping of the years of disturbance and reclamation. The Landsat series of remote-sensing data were used to generate an annual NDVI index that characterizes the annual changes in pixels by constructing long-term annual pixel trajectories.

Timely reclamation following disturbances to land and vegetation is the key to ensuring green mining and sustainable mining [41]. At the national level, it is also hoped that mining and reclamation can be conducted concurrently [42]. However, most mining companies are principally concerned about the efficiency of their mining operations, and so neglect land reclamation and ecological

restoration. Therefore, accurate and timely monitoring of areas of damaged and reclaimed land is particularly important. The method described in this paper achieves rapid and efficient extraction of the spatiotemporal processes of open-pit coal mining and reclamation, thus providing basic data for safe and sustainable mining production and land reclamation. The results of this study may also come to play a crucial role in monitoring and evaluating the implementation of land reclamation.

2. Materials and Methods

2.1. Study Area

Open-pit mining is a driving force for changes in land cover, leading to the loss of natural vegetation and topsoil as well as disruption of ecosystem service flows. In the 21st century, mining has gradually decreased in North America and Europe, but has expanded in South America (including Chile and Brazil) and Asia (including India and China). In the latter regions, the proportion of open-pit mining sites has increased significantly [43]. Surface mining is mining on the ground in which the soil and rock over the mineral deposits are removed. This contrasts with underground mining, in which the overlying rock is left in place and the mineral is removed via shafts or tunnels. The area chosen for this study lies on the eastern plateau of Inner Mongolia, where surface mining has severely disturbed the grassland vegetation. In open-pit mining, the process of disturbing the surface includes stripping of overlying strata, coal-seam mining, solid backfilling, return of top soil, and reclamation.

The study area consisted of the Shengli Coalfield, which is located in Zhenglanqi, to the northwest of Xilingol City, in the Inner Mongolia Autonomous Region (43°54′15″–44°13′52″N, 115°24′26″–116°26′30″E) of China (Figure 1). The terrain of the study area is a gentle undulating piedmont plain, while the climate is that of a semi-arid steppe, with an average temperature of 1.7 °C, a maximum temperature of 38.3 °C, and a minimum temperature of −42.4 °C. The rainfall there averages 294.7 mm a year; the maximum rainfall is 481.0 mm, the minimum rainfall is 146.7 mm, and the average annual evaporation is 1794.6 mm. The area is usually windy in the spring, with wind speeds of 2.1–8.4 m·s^{-1} and an average annual wind speed of 3.5 m·s^{-1}. The soil types there are chestnut calcareous soil, meadow calcareous soil, and meadow soil. Desertified, gravelly calcareous soil has been formed due to grassland degradation. The soil organic matter content is low and the soil fertility is poor. There are two coal-bearing sections in the Shengli Coalfield: the lower coal section of the Cretaceous Bayanhua Group Xilin Formation and the Shengli Formation coal-bearing section. There are seven coal mining groups, with an average burial depth of 200–500 m and an average thickness of 8–60 m. In 1989, the proven and retained reserves were 15.932 billion tons and 15.931 billion tons, respectively.

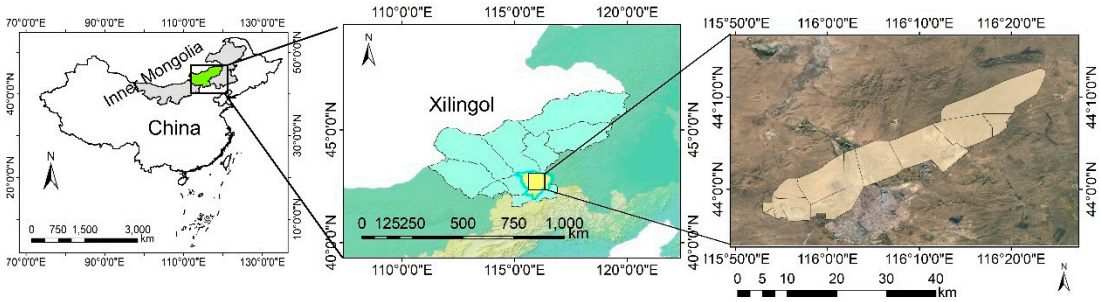

Figure 1. Maps showing the location of the study area in Xilingol, Inner Mongolia, China.

Under the temperate continental climate of the region, this vulnerable natural ecosystem is typical of temperate semi-humid and semi-arid steppes. The area is an important source of green agricultural and livestock products in China. There are 13,786 km^2 of high-quality natural grasslands available in the region. The average vegetation growth season is 141 days, which includes the period from May through September [44]. Vegetation coverage is usually maintained at 40% throughout the year [45].

2.2. Overview of the Methodology

Our methodology is based on the premise that open-pit mining and reclamation activity will cause abrupt changes to vegetation, which can be shown by the trajectory of the vegetation indices. As shown in Figure 2a, there are three main vegetation time series trajectories of pixels in the study area, which represent areas that are undisturbed, disturbed and reclaimed, and disturbed without reclamation. Time series analysis was used to find breakpoints in the trajectories, thereby indicating sudden changes: surface mining including strip mining, open-pit mining, and mountaintop removal mining. In the surface mining process, soil and rock overlying the mineral deposits (the overburden) are removed, and the vegetation is disturbed in this process. During overburden removal, substantial vegetation is disturbed by both stripping and dumping (second curve in Figure 2a). The dumps are subsequently reclaimed and revegetated, and the open-pit is covered by topsoil and revegetated following mining activities (third curve in Figure 2a). The aforementioned process includes vegetation disturbance and reclamation. According to our field study, natural recovery usually takes more than three years; thus, these sudden changes within two years can be considered to be caused by human activities.

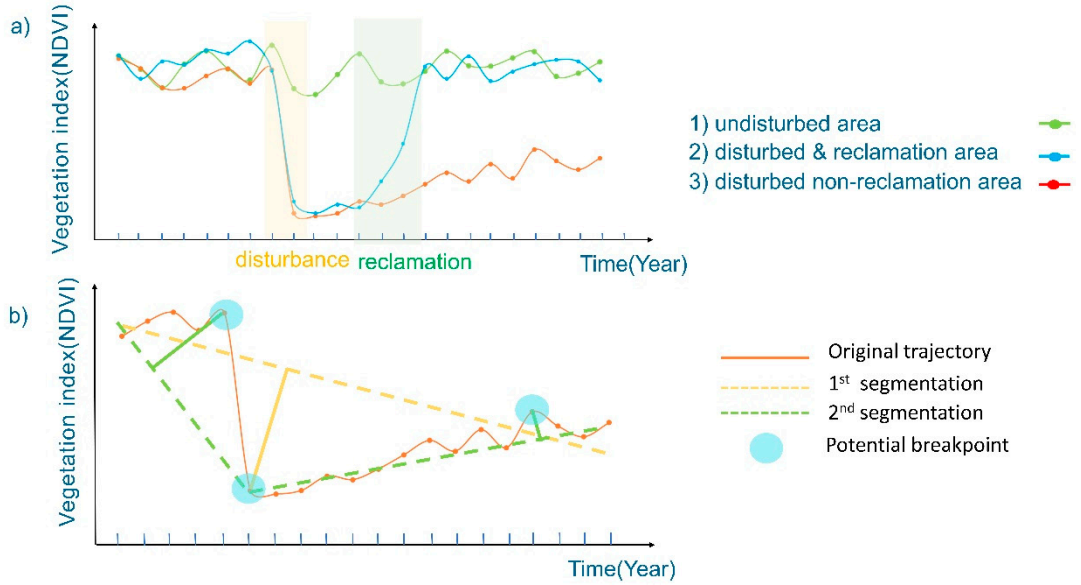

Figure 2. (**a**) Three types of pixel-based annual vegetation index curves: (1) undisturbed pixels, (2) pixels with mining disturbances and no reclamation efforts, and (3) pixels with mining disturbances and land reclamation. (**b**) Conception map of LandTrendr line segmentation.

The LandTrendr algorithm was used to find breakpoints; a simple concept map based on the work of Kennedy et al. [35] is shown in Figure 2b. This process of line segmentation was guided by the curve itself, and then the actual breakpoints among the potential breakpoints were decided according to the parameter settings.

The entire process is shown in Figure 3 and has two main components: (i) disturbance to the vegetation of the surface mining area and detection of reclamation and (ii) accuracy verification. First, Landsat surface reflection data were preprocessed by masking snow and cloud cover. Then the 2003–2019 sequence image collection was processed to form the annual 95th percentile NDVI. The selection of Landsat images for the entire period avoided manual selection and shadow accumulation errors. The annual 95th percentile NDVI was then used to reduce vegetation index extraction errors caused by the selection of specific time nodes and to facilitate the analysis of this vegetation disturbance and reclamation process in a more efficient and time-saving manner. Finally, spatiotemporal information about sudden changes in the NDVI time series was gained from using the LandTrendr algorithm. In the accuracy verification, we picked sample points from areas where changes were detected and validated them with the images obtained from Google Earth.

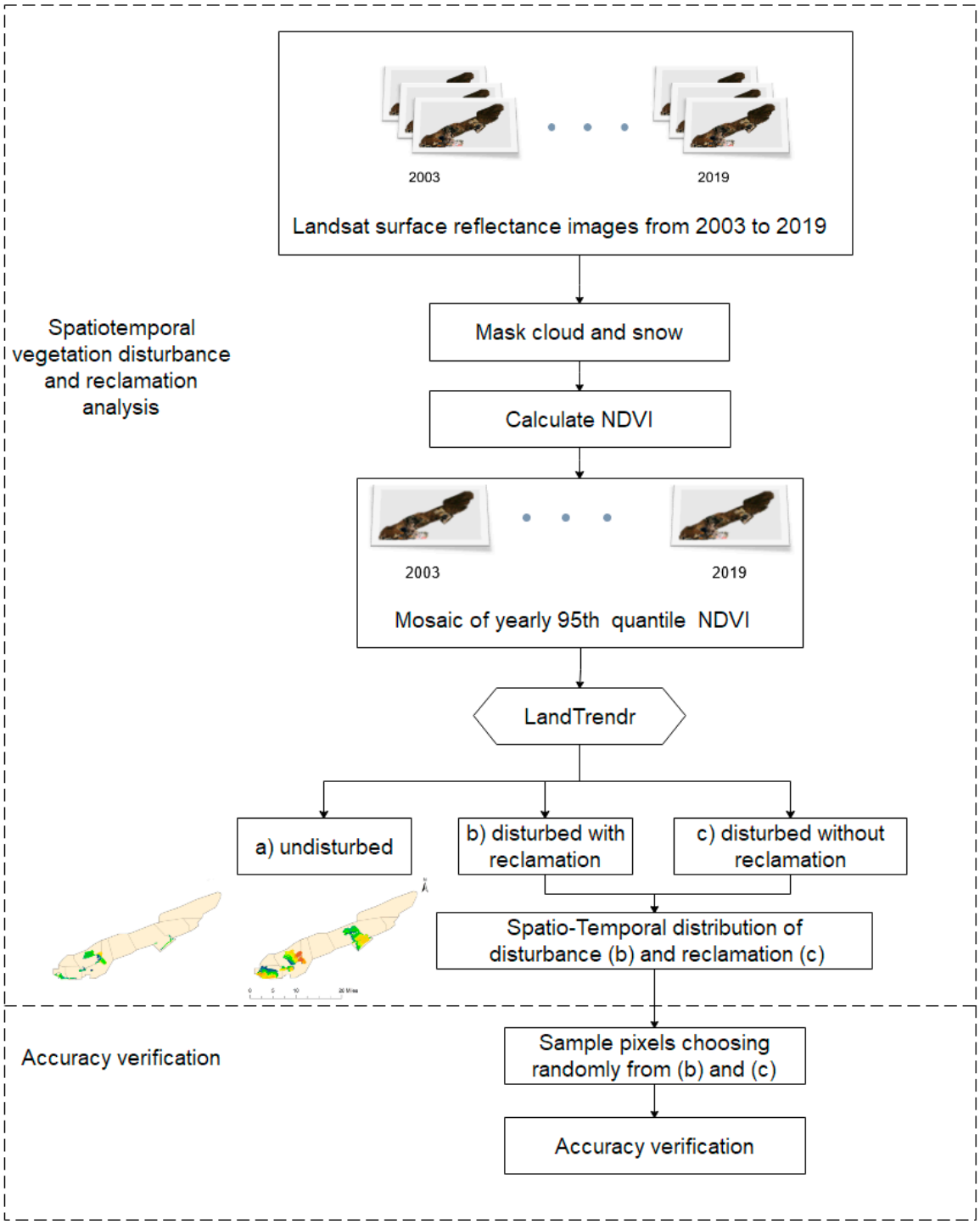

Figure 3. Workflow of the methodology used in this study.

2.3. Data Acquisition and Preprocessing

This study selected all of the Landsat surface reflectance (SR) images on the GEE platform from 1 January 2001 through 30 December 2019, including images from Landsat 5, 7, and 8. The Landsat SR data from the GEE platform had already had the Landsat Ecosystem Disturbance Adaptive Processing System (LEDAPS) atmosphere correction applied. The number of SR images available for the study area for the period from 2001 through 2019 is shown in Figure 4a. Using the quality assessment (QA) band to indicate the possibilities of cloud, cloud shadow, snow, etc., in each pixel, the cloud, cloud

shadow, and snow pixels were masked. The number of remaining valid images in each pixel of the study area is shown in Figure 4b. In this way, the synthesis of good observations produced a collection of cloud-free SR images for each year [46] for subsequent processing.

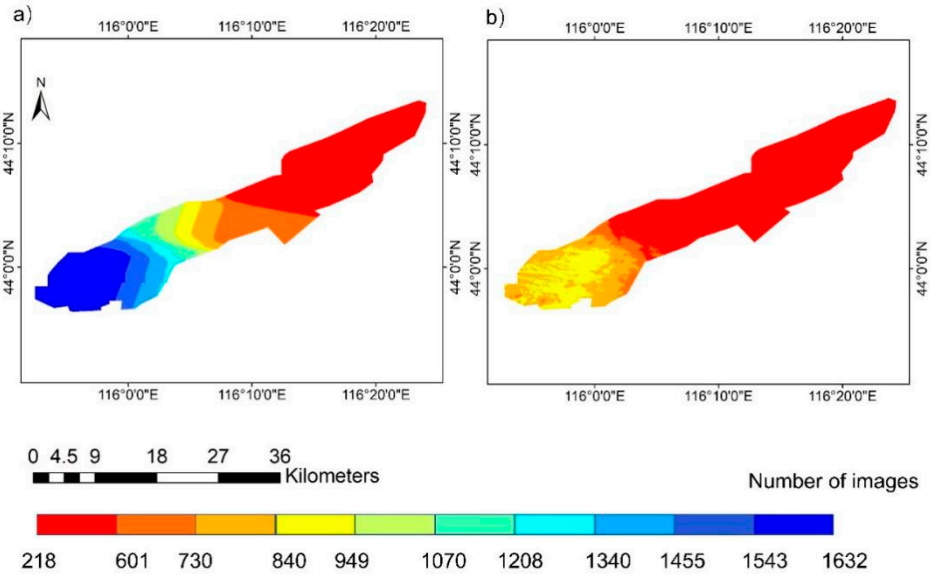

Figure 4. Distribution of available images and good observations in the study area between 2001 and 2019. (**a**) All surface reflectance (SR) data and (**b**) good observations after masking clouds, cloud shadows, and snow.

The collection of good observations was then ready to generate a collection of 20 images (2003–2019) with a specified index indicating changes that required observation. A previous study by Karan showed that NDVI was the best indicator for detecting changes in coal mine vegetation [47]. Thus, we used the NDVI to represent vegetation growth. The NDVI was calculated as follows:

$$NDVI = (\rho_{\text{NIR}} - \rho_{\text{Red}})/(\rho_{\text{Red}} + \rho_{\text{NIR}}) \quad (1)$$

where ρ_{Red} and ρ_{NIR} are the surface reflection values in the red and infrared bands, respectively.

The annual phenology curves of vegetated pixels differ from year to year, but some characteristics of the curve, such as peaks, can indicate the growth of vegetation. We then used the 95th percentile NDVI to represent the growth of vegetation for that year. Finally, the 2001–2019 image collection comprised of 20 images was ready for time series fitting analysis using the LandTrendr algorithm.

2.4. Identification of Disturbance and Reclamation Years

Mining activity includes land cover removal, overburden dumps, and construction that causes the natural environment to abruptly change to barren land or a structure [48]. Various reclamation strategies can be used to seek recovery of vegetation and restoration of ecological function [49]. These reclamation processes usually require months or even years, while mining itself results in relatively fast, severe losses of vegetation. Reclamation leads to faster and greater vegetation recovery than natural processes driven by climate, and is thus suitable for measurement via interannual vegetation changes. As shown in Figure 2, the mining disturbance date of a pixel occurred when an abrupt minimum NDVI was observed, and the reclamation date occurred when vegetation recovery suddenly increased and stabilized.

The LandTrendr algorithm, with its GEE version available online according to Kennedy et al. [50], uses an iterative calculation that includes continuous determination of breakpoints and fitting based on the time series trajectory of a single 30 m × 30 m Landsat image pixel. Breaks are set according to particular parameter values, such as identified mutation types, the maximum number of breakpoints,

etc. Different parameters did not affect the result; thus, default parameters were used to simplify the workflow. Each pixel in the resulting image had a matrix indicating whether there had been an abrupt change and, if so, when it changed. By choosing vegetation loss, information about the spatiotemporal distribution of vegetation disturbance occurring in the mining area was gained. Pixels for a sudden increase in vegetation were also obtained. These points were determined and are shown on the map, along with the time of the abrupt change. The mining and reclamation years were determined based on the assumptions that vegetation loss represented mining and that vegetation gain represented reclamation. Thus, maps of vegetation damage and vegetation restoration caused by mining and reclamation, respectively, were generated.

2.5. Data Post-processing, Accuracy Assessment, and Validation

The results of our study indicate that disturbances occurred in the period from 2004–2019 and reclamation occurred in the period from 2007–2019. Thus, we randomly selected 50 points in the disturbance area and 30 points in the reclamation area for each year. This produced a total of 800 disturbance and 390 reclamation sample points. Then, we used the high-resolution image data on Google Earth to perform interactive visual calibrations and determine the disturbance and recovery years of each sample point. By comparing the sample label with the algorithmic identification results, the user, producer, overall accuracy, and kappa coefficients for mining disturbance and reclamation monitoring were calculated, as described in the next section.

3. Results

3.1. Disturbance and Reclamation Accuracy Assessment

There were 26,153 identified reclamation pixels, of which 25,905 (99.05%) were disturbed. The overall accuracies of vegetation disturbance and reclamation date (year) identification were 0.84 and 0.81, and the kappa coefficients were 0.83 and 0.79, respectively (Figure 5). Thus, the overall disturbance and reclamation recognition accuracies were found to be quite good.

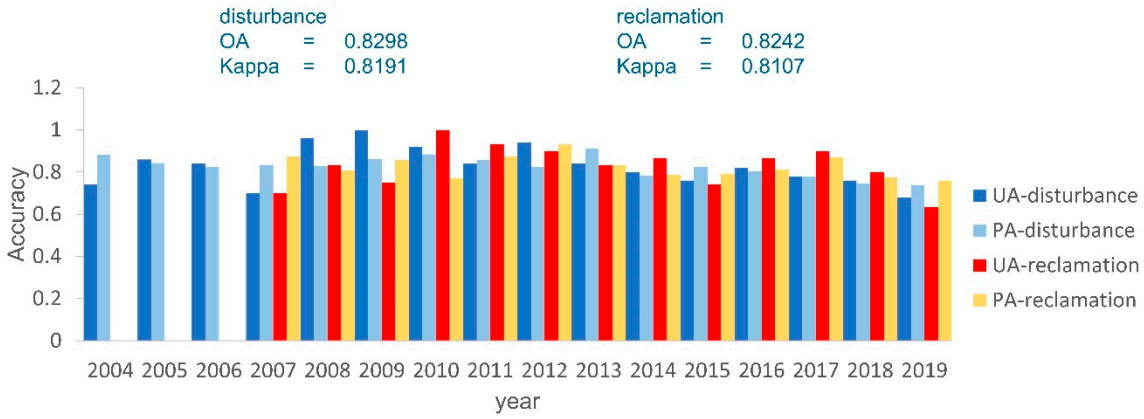

Figure 5. Accuracy of disturbance and reclamation year identification between 2003 and 2019. Accuracies of the disturbance and reclamation years: PA: producer accuracy; UA: user accuracy; OA: overall accuracy.

3.2. Spatiotemporal Characteristics of Vegetation Changes

The spatiotemporal mapping of the mining disturbance and reclamation years is shown in Figures 6 and 7. There are three main mining areas in the Shengli Coalfield, which are circled in red in the figures. Figures 6 and 7 each include a year map of human activity (Figures 6a and 7a), an enlarged map of the three main mining areas (Figures 6b and 7b), and a time series of a region representing the typical tracks of mining and reclamation, respectively, with high-resolution Google Earth images below the trajectory (Figures 6c and 7c).

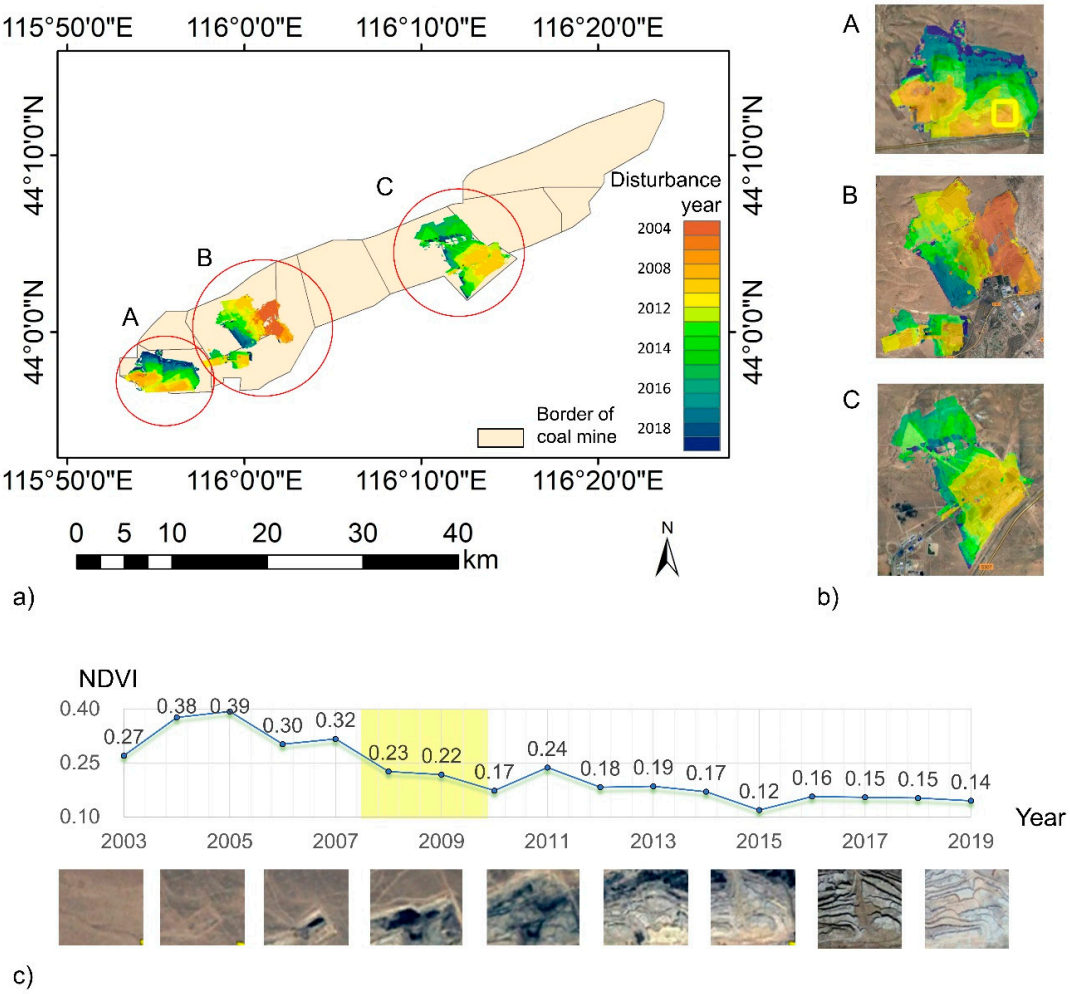

Figure 6. (**a**) Spatiotemporal map of 2004–2019 mining disturbances in the study area; (**b**) spatiotemporal disturbance map of the three main mining areas of the Shengli Coalfield (labeled as A, B, C in (a)); and (**c**) time series curve and high-resolution satellite image of the area indicated by the yellow frame in the mining area marked B in (b).

According to the results of our study, large-scale mining began after 2007, while most recovery processes occurred after 2011. Reclamation and mining activities both show spatial patterns of starting on one side of the mine and gradually advancing.

Figure 8a is a histogram representing the area disturbed and reclaimed each year in the study area. It is worth noting that mining activity has decreased since 2014 and reclamation activity has become more concentrated since 2011. In Figure 8b, the cumulative mining and reclamation areas are shown in the cumulative area chart, and the yearly reclamation rate is drawn as a line chart, with a specific number noted above the curve. The area of cumulative mining minus that of reclamation reaches a dynamic balance after 2010 due to reclamation commencing. A significant rise in the reclamation rate during 2010–2011 is evident, and the reclamation rate stabilizes at 25% after 2014.

We further investigated the mining and reclamation time of each pixel and counted the number of pixels in different time periods. According to the statistics presented in Table 1, in which the reclamation year is given horizontally and the vegetation disturbance year (caused by mining activity) is given vertically, 99,982 pixels were disturbed between 2003 and 2019, accounting for approximately 90 km^2. During the same period, 26,153 pixels were monitored for reclamation, accounting for approximately 24 km^2. Of these, 25,948 pixels were previously detected as disturbed, with a drastic decline in vegetation coverage, while 205 pixels were not. The latter group may be reclamation pixels that did not experience any severe disturbance. It is evident that the earlier the mining started, the higher the

proportion of land reclamation. For example, 90% of the area subjected to vegetation loss caused by mining activities in 2004 has been recovered, while less than 10% of the area disturbed after 2012 has been repaired.

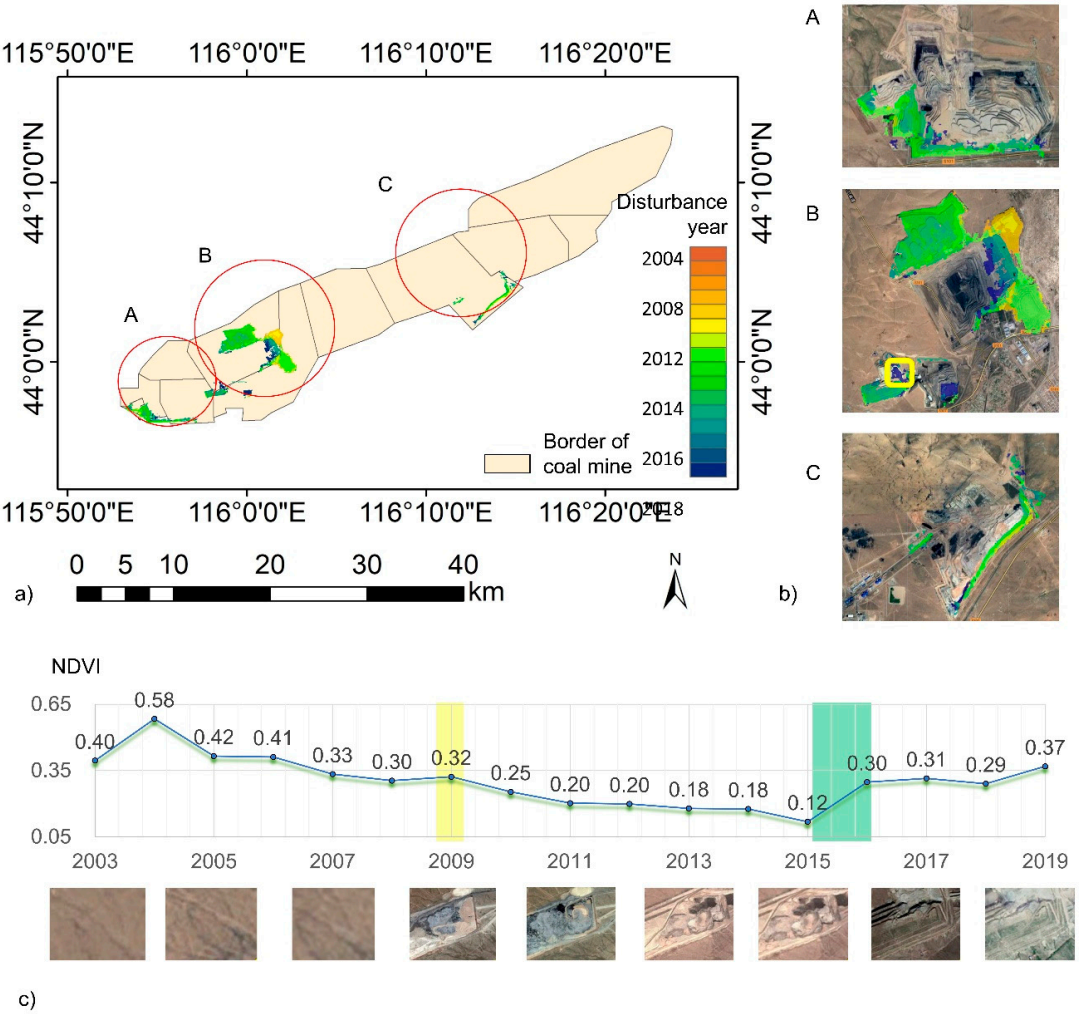

Figure 7. (**a**) Spatiotemporal map of reclamation from 2007 through 2019 in the study area; (**b**) spatiotemporal reclamation map of the three main mining areas of the Shengli Coalfield (labeled as A, B, C in (a)); and (**c**) time series curve and high-resolution satellite image of the area indicated by the yellow frame in the mining area marked A in (b).

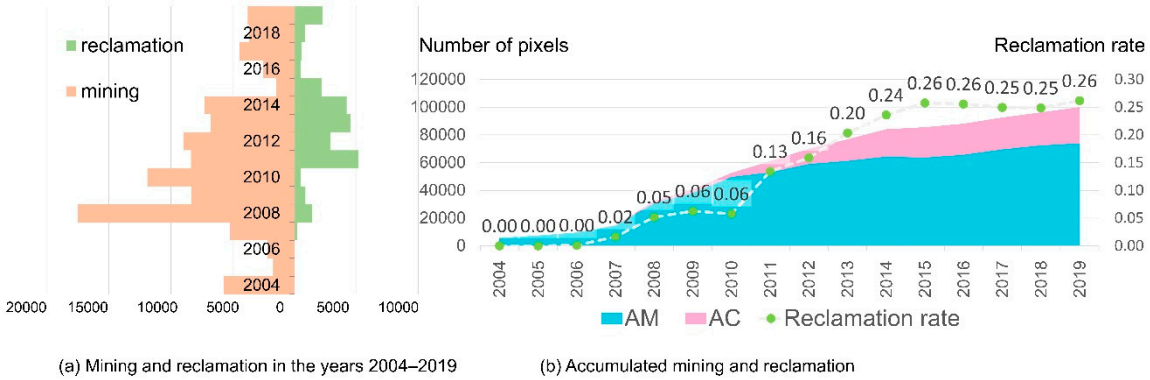

Figure 8. Statistical map of mining and reclamation. (**a**) Number of mining and reclamation pixels for each year and (**b**) number of mining and reclamation pixels accumulated through each year. The yearly reclamation rate is noted. AM: accumulated mining area; AC: accumulated reclamation area.

Table 1. Number of pixel changes for various disturbance and reclamation years. The year of reclamation is given horizontally, while the year of disturbance (mining activity) is given vertically.

Year	2006	2007	2008	2009	2010	2011	2012	2013	2014	2015	2016	2017	2018	2019	UP	RM
2004	11	104	1018	623	24	1135	120	44	37	651	254	363	274	551	529	0.91
2005	0	128	97	66	0	326	93	7	12	62	5	34	55	198	656	0.62
2006	0	0	305	60	7	992	125	19	56	20	1	0	11	2	570	0.74
2007	0	0	7	75	91	1379	196	265	386	261	16	27	59	69	2384	0.54
2008	0	0	0	54	362	684	944	1174	800	495	9	35	119	495	12,345	0.30
2009	0	0	0	1	5	390	687	1084	952	354	21	50	126	182	4497	0.46
2010	0	0	1	1	0	214	688	1266	1081	132	26	10	40	0	8235	0.30
2011	0	0	0	0	0	0	62	638	448	37	1	3	11	83	7087	0.15
2012	0	0	0	0	0	0	1	11	388	144	91	13	53	152	8141	0.09
2013	0	0	0	0	0	0	1	0	37	39	44	24	6	126	6500	0.04
2014	0	0	0	0	0	0	0	0	0	6	16	4	77	48	7118	0.02
2015	0	0	0	0	0	0	1	0	0	0	0	0	0	0	1482	0.00
2016	0	0	0	0	0	1	1	0	5	0	0	0	3	14	2522	0.01
2017	0	0	0	0	0	0	0	0	0	0	0	0	0	115	4328	0.03
2018	0	0	0	0	0	8	3	0	0	2	0	0	0	8	3675	0.01
2019	0	0	0	0	0	10	0	1	4	0	0	0	2	1	3762	0.00

Note: UP indicates the number of unchanged pixels, i.e., those that underwent mining without reclamation, while RM indicates the percentage of pixels that were reclaimed in a later period after being mined in a particular year.

The information in Table 1 can be visualized using Figure 9, which shows a pixel reclamation matrix for various years. The following characteristics are most noticeable: those pixels disturbed during the period from 2007–2011 have been reclaimed in large numbers in the period from 2011–2014. The reclamation chart of the region forms a triangle in the picture. In addition, reclamation performed in 2011 covers mining from 2004 through 2008. Finally, it can be seen that the pixels mined in 2004 have been reclaimed for many years until 2019.

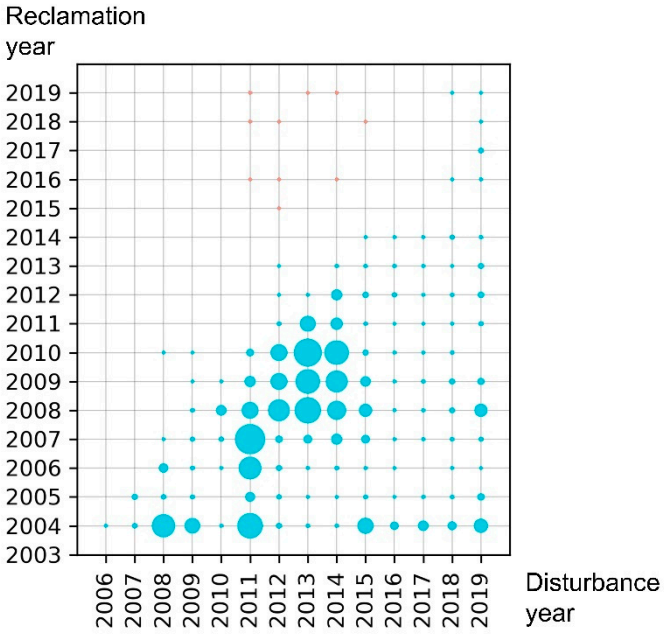

Figure 9. Map showing the number of pixels reclaimed following mining. The number of pixels in each combination of mining and reclamation year is indicated by the size of the blue dot if the mining year is earlier than the reclamation year, or else by the size of a red dot.

4. Discussion

The grasslands of Inner Mongolia are rich in coal. Their delicate ecosystems have been threatened by increased mining activity as a result of the depletion of the coal resources of other provinces following years of mining [51]. The developing Shengli Coalfield in Xilingol was chosen as the study area for examination of yearly mining and reclamation activities, an area that has been the subject of numerous studies, varying from the impacts of mining and reclamation on vegetation dynamics to their impacts on the landscape [52]. Utilizing the GEE platform and the LandTrendr algorithm, our methodology was used to determine the spatiotemporal distributions of mining and reclamation rapidly, accurately, and with high spatial resolution (30 m). One benefit of applying this methodology to open-pit mining is that it is an unsupervised process, unlike time series filtering and classification, which require sample training [53] and integrated clustering of pixel classification [54]. It is also worth noting that the use of SR data and operations on image collections enable one to examine mining and reclamation situations where grassland is the original vegetation. Other disturbance and reclamation detection projects have used similar methods in forested areas [40,55]. If the year map on which pixels detect disturbances and reclamation appears to be clustered rather than discrete, this indicates that there are massive mining or reclamation activities. This method can be applied to the open-pit coal mines in the steppe area and can detect the mining and reclamation years over long periods of time.

4.1. Applicability of the Method

The mining of open pits is often accompanied by the destruction of vegetation, which causes a sudden reduction in the vegetation index. Therefore, time series change monitoring and the LandTrendr algorithm can be used to determine the year when the quantity of vegetation changed

abruptly. The NDVI is more robust than other vegetation indices, such as the EVI in grasslands, and the 95th percentile of the annual NDVI can reflect vegetation growth in that year quite well [56]. It can be used broadly in areas that exhibited vegetation coverage before open-pit mining began. This algorithm is based on the GEE web platform, which has almost no computing requirements and is easy to transfer.

4.2. Comparison with Existing Products

Using the information on vegetation disturbance years presented in this paper, it is possible to generate a map of vegetation changes for any time period in the study area. In addition, comparing multiphase images is a traditional method for detecting vegetation changes in open-pit mines. We used the National Land Cover Database (NLCD) data set to generate vegetation change maps from 2010 through 2018 [57]. It should be noted that NLCD is a product that is interpreted manually and cannot be used as a factual basis. For direct comparison, in Figure 6c, we chose a rectangular area of 4 km × 5 km. The results show that the area of reduced vegetation from NLCD products is greater than the results presented in this paper. Moreover, the image spots of the NLCD products are more concentrated, mainly because NLCD is an object-oriented manual interpretation product and the algorithm used in this study is pixel-based. Thus, it is difficult to avoid the salt-and-pepper noise phenomenon [58]. However, our results detected more details: the vegetation in the black ellipse in Figure 10 has not been significantly reduced, but NLCD mistakenly identified it as vegetation. In addition, the blue ellipse in Figure 10 shows that the vegetation disturbance boundary identified by results in this study is more similar to the original image of the boundary of topsoil stripping due to mining. For this reason, the method of detecting vegetation disturbance put forward in this paper is superior to the traditional comparative method.

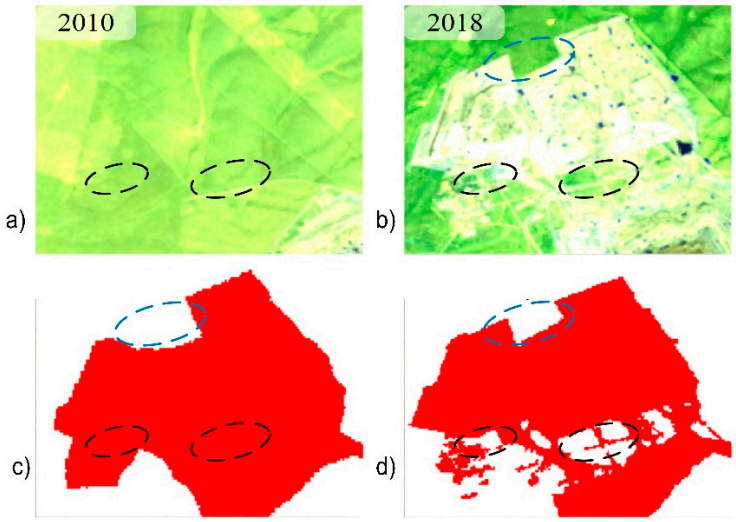

Figure 10. Vegetation disturbance mapping results of a typical region (4 km × 5 km) in the period from 2010–2018. (**a**) A false color composite image with a band combination of 7/5/3 (R/G/B) of Landsat 5 surface reflection data in 2010; (**b**) A false color composite image with a band combination of 7/6/4 (R/G/B) of Landsat 8 surface reflection data in 2018; (**c**) disturbance area mapping results from the National Land Cover Database (NLCD) data set; (**d**) disturbance area mapping results in this study.

4.3. Method Defects and Generalization

The defects in and prospects for generalization of this methodology are discussed primarily from three angles: applicable objectives, algorithmic operability, and accuracy. This method can be applied to detect mining and reclamation activity in open-pit mines. As for underground mining, subsidence caused by mining does not usually disturb the vegetation, and thus is hard to monitor from the surface. With regard to algorithmic operability, adjusting the algorithm in the GEE platform is relatively simple. However, pixel-based algorithms usually have accuracy problems. As shown in

Table 1, there are 41 pixels that were incorrectly identified, with their reclamation year earlier than their mining year. A few pixels outside the main mining area were detected as disturbed or reclaimed. We can erase such pixels via eight-field smoothing. In addition, there are some undetected pixels. These types of errors are common in pixel-based algorithms due to salt-and-pepper noise and other causes. Moreover, we used this method in a specific mining region, which means that the mining boundary was identified prior to analysis. Thus, how to implement the proposed method for an area with an unknown mining boundary and avoid the impacts resulting from urbanization and related vegetation disturbance requires more work to be done.

4.4. Implications for Ecological Monitoring and Reclamation

The methodology that we have pioneered can identify effectively areas newly subject to reclamation and mining, as well as the net area that is destroyed (the cumulative reclamation area minus the cumulative mining area) each year. Figure 8b shows that the areas of cumulative damage by mining changed little after 2010, as the area already disturbed but not reclaimed tended to vary slowly, with few fluctuations. This reflects the effectiveness of reclamation and the dynamic balance that can be maintained by conducting reclamation while continuing mining activities. This serves to protect the environment and maintain the original ecosystem functions. The results extracted by the algorithm indicate clear monitoring of mining disturbance and reclamation. This algorithm can play a role in monitoring vast areas for mine reclamation in the future. At the enterprise level, the use of this algorithm for rapid and extensive nonmanual monitoring is low-cost, and can be combined with direct observation of land reclaimed from mining. It may enable a quantitative understanding of the effects of mining and reclamation, and allow the exploration of more efficient reclamation methods. Nevertheless, further specific analyses need to be performed in order to explore the mechanisms and impacts of mining activities, such as comparisons with the data for annual coal production [59] and various analyses of vegetation dynamics that address the impacts of mining on the health of ecosystems [60].

5. Conclusions

China's coal consumption is substantial, and the output of coal mines is indispensable to economic development. Pressure from environmental and energy needs, however, means that coal mines must be transformed. Open-pit mines produce extensive surface damage, and application of soil reconstruction and vegetation reclamation is especially important. To this end, we proposed a method of rapid, large-scale mining and reclamation monitoring to improve oversight of the changes resulting from open-pit mining. This can help us to understand the natural vegetation recovery mechanisms in disturbed areas without reclamation, as well as the reclamation status of reclaimed areas.

The current GEE-based algorithms are fast and effective, and are increasingly the preferred means of performing remote-sensing research. The method described in this paper monitored mining and reclamation in the Shengli open-pit mining area effectively. The disadvantage of this pixel-based method is that it lacks neighborhood information, and thus is not helpful for identifying sources of sudden interference. Reasonable explanations can be obtained only in limited scenarios, such as those of the mining and reclamation activities described in this paper. In the future, we may integrate object-oriented mining and reclamation monitoring methods and compare the results with pixel-based algorithms.

Author Contributions: Conceptualization, W.X. and T.H.; methodology, W.X., T.H., and X.D.; software, T.H.; validation, W.X., W.C., and T.H.; formal analysis, W.C.; investigation, W.X.; data curation, T.H. and X.D.; writing—original draft preparation, W.X., X.D., and T.H.; writing—review and editing, X.D. and W.C.; visualization, T.H.; supervision, W.X.; project administration, W.X.; funding acquisition, W.X. All authors have read and agreed to the published version of the manuscript.

Funding: This work was supported by the National Key Research and Development Program of China (2016YFC0501103).

Conflicts of Interest: The authors declare that they have no conflict of interest.

References

1. Xiao, W.; Lv, X.J.; Zhao, Y.L.; Sun, H.X.; Li, J.Q. Ecological resilience assessment of an arid coal mining area using index of entropy and linear weighted analysis: A case study of Shendong Coalfield, China. *Ecol. Indic.* **2020**, *109*, 105843. [CrossRef]
2. Lv, X.J.; Xiao, W.; Zhao, Y.L.; Zhang, W.K.; Li, S.C.; Sun, H.X. Drivers of spatio-temporal ecological vulnerability in an arid, coal mining region in Western China. *Ecol. Indic.* **2019**, *106*, 105475. [CrossRef]
3. Schladweiler, B.K. 40 years of the Surface Mining Control and Reclamation Act(SMCRA): What have we learned in the State of Wyoming. *Int. J. Coal Sci. Technol.* **2018**, *5*, 3–7. [CrossRef]
4. Wu, B.; Zhao, Y.; Fang, C. Detection of Spatiotemporal Changes of Surface Mining Area in Changting County Southeast China. In Proceedings of the IGARSS 2019–2019 IEEE International Geoscience and Remote Sensing Symposium, 28 July–2 August 2019; pp. 1606–1609.
5. Ahirwal, J.; Maiti, S.K. Assessment of soil properties of different land uses generated due to surface coal mining activities in tropical Sal (Shorea robusta) forest, India. *Catena (Amst)* **2016**, *140*, 155–163. [CrossRef]
6. Kompala-Baba, A.; Sierka, E.; Dyderski, M.K.; Bierza, W.; Magurno, F.; Besenyei, L.; Blonska, A.; Rys, K.; Jagodzinski, A.M.; Wozniak, G. Do the dominant plant species impact the substrate and vegetation composition of post-coal mining spoil heaps? *Ecol. Eng.* **2020**, *143*, 105685. [CrossRef]
7. Xiao, W.; Fu, Y.H.; Wang, T.; Lv, X.J. Effects of land use transitions due to underground coal mining on ecosystem services in high groundwater table areas: A case study in the Yanzhou coalfield. *Land Use Policy* **2018**, *71*, 213–221. [CrossRef]
8. Pettorelli, N.; Vik, J.O.; Mysterud, A.; Gaillard, J.M.; Tucker, C.J.; Stenseth, N.C. Using the satellite-derived NDVI to assess ecological responses to environmental change. *Trends Ecol. Evol.* **2005**, *20*, 503–510. [CrossRef]
9. Islam, K.; Vilaysouk, X.; Murakami, S. Integrating remote sensing and life cycle assessment to quantify the environmental impacts of copper-silver-gold mining: A case study from Laos. *Resour. Conserv. Recycl.* **2020**, *154*, 104630. [CrossRef]
10. Lein, J.K. Implementing remote sensing strategies to support environmental compliance assessment: A neural network application. *Environ. Sci. Policy* **2009**, *12*, 948–958. [CrossRef]
11. Chen, W.T.; Li, X.J.; He, H.X.; Wang, L.Z. Assessing Different Feature Sets' Effects on Land Cover Classification in Complex Surface-Mined Landscapes by ZiYuan-3 Satellite Imagery. *Remote Sens.* **2018**, *10*, 23. [CrossRef]
12. Li, X.J.; Chen, W.T.; Cheng, X.W.; Wang, L.Z. A Comparison of Machine Learning Algorithms for Mapping of Complex Surface-Mined and Agricultural Landscapes Using ZiYuan-3 Stereo Satellite Imagery. *Remote Sens.* **2016**, *8*, 514. [CrossRef]
13. Wen, B.; Pan, Y.H.; Zhang, Y.Y.; Liu, J.J.; Xia, M. Does the Exhaustion of Resources Drive Land Use Changes? Evidence from the Influence of Coal Resources-Exhaustion on Coal Resources-Based Industry Land Use Changes. *Sustainability* **2018**, *10*, 2698. [CrossRef]
14. Zhang, X.D.; Ge, D.Q.; Wu, L.X.; Zhang, L.; Wang, Y.; Guo, X.F.; Li, M.; Yu, X.G. Study on monitoring land subsidence in mining city based on coherent target small-baseline InSAR. *J. China Coal Soc.* **2012**, *37*, 1606–1611.
15. Li, J.; Jiao, L.; Shen, Y.; Liu, Q. Land use and cover change in coal mining area by IFZ and NDVI. *J. China Coal Soc.* **2016**, *41*, 2822–2829.
16. Li, J.; Cui, L.; Yan, X.; Yang, Z.; Dong, J.; Deng, X. Comparative analysis of long-term trends on fraction of vegetation coverage in grassland mining area. *Bull. Surv. Mapp.* **2019**, *8*, 130–134.
17. Jia, D.; Shouguo, M.U.; Zhao, H. Analysis of NDVI Time Series in Grassland Open-cast Coal Mines Based on SSA-Mann Kendall. *Int. J. Geogr. Inf. Sci.* **2016**, *18*, 1110–1122.
18. Li, H.; Lei, J.; Wu, J. Analysis of land damage and recovery process in rare earth mining area based on multi-source sequential NDVI. *Trans. Chin. Soc. Agric. Eng.* **2018**, *34*, 232–240.
19. Snapir, B.; Simms, D.M.; Waine, T.W. Mapping the expansion of galamsey gold mines in the cocoa growing area of Ghana using optical remote sensing. *Int. J. Appl. Earth Obs. Geoinf.* **2017**, *58*, 225–233. [CrossRef]
20. Demirel, N.; Emil, M.K.; Duzgun, H.S. Surface coal mine area monitoring using multi-temporal high-resolution satellite imagery. *Int. J. Coal Geol.* **2011**, *86*, 3–11. [CrossRef]

21. Latifovic, R.; Fytas, K.; Chen, J.; Paraszczak, J. Assessing land cover change resulting from large surface mining development. *Int. J. Appl. Earth Obs. Geoinf.* **2005**, *7*, 29–48. [CrossRef]
22. Erener, A. Remote sensing of vegetation health for reclaimed areas of Seyitomer open cast coal mine. *Int. J. Coal Geol.* **2011**, *86*, 20–26. [CrossRef]
23. Obade, V.D.; Lal, R. Assessing land cover and soil quality by remote sensing and geographical information systems (GIS). *Catena (Amst)* **2013**, *104*, 77–92. [CrossRef]
24. Townsend, P.A.; Helmers, D.P.; Kingdon, C.C.; McNeil, B.E.; de Beurs, K.M.; Eshleman, K.N. Changes in the extent of surface mining and reclamation in the Central Appalachians detected using a 1976–2006 Landsat time series. *Remote Sens. Environ.* **2009**, *113*, 62–72. [CrossRef]
25. Matejicek, L.; Kopackova, V. Changes in Croplands as a Result of Large Scale Mining and the Associated Impact on Food Security Studied Using Time-Series Landsat Images. *Remote Sens.* **2010**, *2*, 1463–1480. [CrossRef]
26. Li, J.; Zipper Carl, E.; Li, S.; Donovan Patricia, F.; Wynne Randolph, H.; Oliphant Adam, J.; Xia, Q. Character analysis of mining disturbance and reclamation trajectory in surface coal-mine area by time-series NDVI. *Trans. CSAE* **2015**, *31*, 251–257.
27. Yang, Z.; Li, J.; Zipper, C.E.; Shen, Y.Y.; Miao, H.; Donovan, P.F. Identification of the disturbance and trajectory types in mining areas using multitemporal remote sensing images. *Sci. Total Environ.* **2018**, *644*, 916–927. [CrossRef]
28. Gorelick, N.; Hancher, M.; Dixon, M.; Ilyushchenko, S.; Thau, D.; Moore, R. Google Earth Engine: Planetary-scale geospatial analysis for everyone. *Remote Sens. Environ.* **2017**, *202*, 18–27. [CrossRef]
29. Zhang, T.; Tang, H. Vegetation Cover Change and Urban Expansion in Beijing-Tianjin-Hebei during 2001~2015based on Google Earth Engine. *Remote Sens. Technol. Appl.* **2018**, *33*, 593–599.
30. Chen, W.; Huang, H.; Tian, Y.; Du, Y. Monitoring and Assessment of the Eco-Environment Quality in the Sanjiangyuan Region based on Google Earth Engine. *Int. J. Geogr. Inf. Sci.* **2019**, *21*, 1382–1391.
31. Bunting, E.L.; Munson, S.M.; Bradford, J.B. Assessing plant production responses to climate across water-limited regions using Google Earth Engine. *Remote Sens. Environ.* **2019**, *233*, 111379. [CrossRef]
32. Hu, Y.F.; Dong, Y.; Batunacun. An automatic approach for land-change detection and land updates based on integrated NDVI timing analysis and the CVAPS method with GEE support. *ISPRS J. Photogramm. Remote Sens.* **2018**, *146*, 347–359. [CrossRef]
33. Zhu, Z. Change detection using landsat time series: A review of frequencies, preprocessing, algorithms, and applications. *ISPRS J. Photogramm. Remote Sens.* **2017**, *130*, 370–384. [CrossRef]
34. Huang, C.; Coward, S.N.; Masek, J.G.; Thomas, N.; Zhu, Z.; Vogelmann, J.E. An automated approach for reconstructing recent forest disturbance history using dense Landsat time series stacks. *Remote Sens. Environ.* **2010**, *114*, 183–198. [CrossRef]
35. Kennedy, R.E.; Yang, Z.G.; Cohen, W.B. Detecting trends in forest disturbance and recovery using yearly Landsat time series: 1. LandTrendr—Temporal segmentation algorithms. *Remote Sens. Environ.* **2010**, *114*, 2897–2910. [CrossRef]
36. Zhu, Z.; Woodcock, C.E. Continuous change detection and classification of land cover using all available Landsat data. *Remote Sens. Environ.* **2014**, *144*, 152–171. [CrossRef]
37. Li, J.; Zipper, C.E.; Donovan, P.F.; Wynne, R.H.; Oliphant, A.J. Reconstructing disturbance history for an intensively mined region by time-series analysis of Landsat imagery. *Environ. Monit. Assess.* **2015**, *187*, 557. [CrossRef]
38. Shen, W.; Li, M.; Huang, C. Review of remote sensing algorithms for monitoring forest disturbance from time series and multi-source data fusion. *J. Remote Sens.* **2018**, *22*, 1005–1022.
39. Zou, Z.H.; Xiao, X.M.; Dong, J.W.; Qin, Y.W.; Doughty, R.B.; Menarguez, M.A.; Zhang, G.L.; Wang, J. Divergent trends of open-surface water body area in the contiguous United States from 1984 to 2016. *Proc. Natl. Acad. Sci. USA* **2018**, *115*, 3810–3815. [CrossRef]
40. Yang, Y.J.; Erskine, P.D.; Lechner, A.M.; Mulligan, D.; Zhang, S.L.; Wang, Z.Y. Detecting the dynamics of vegetation disturbance and recovery in surface mining area via Landsat imagery and LandTrendr algorithm. *J. Clean. Prod.* **2018**, *178*, 353–362. [CrossRef]
41. Krzyszowska Waitkus, A. Surface coal mine permit application for successful reclamation, semi-arid shortgrass prairie (Wyoming, USA)(Article). *Int. J. Coal Sci. Technol.* **2018**, *5*, 8–17. [CrossRef]

42. Ren, H.; Zhao, Y.; Xiao, W.; Hu, Z. A review of UAV monitoring in mining areas: Current status and future perspectives. *Int. J. Coal Sci. Technol.* **2019**, *6*, 320–333. [CrossRef]
43. Yu, L.; Xu, Y.D.; Xue, Y.M.; Li, X.C.; Cheng, Y.Q.; Liu, X.X.; Porwal, A.; Holden, E.J.; Yang, J.; Gong, P. Monitoring surface mining belts using multiple remote sensing datasets: A global perspective. *Ore Geol. Rev.* **2018**, *101*, 675–687. [CrossRef]
44. Wu, R.; Hong, Y.; Bao, G. The Change of Vegetation Phenology and its Impacts on Vegetation Productivity in Inner Mongolia during 20012016. *Acta Agrestia Sin.* **2019**, *27*, 1685–1693.
45. Mu, S.; Yang, H.; Li, J.; Chen, Y.; Gang, C.; Zhou, W.; Ju, W. Spatio-temporal dynamics of vegetation coverage and its relationship with climate factors in Inner Mongolia, China. *J. Geogr. Sci.* **2013**, *23*, 231–246. [CrossRef]
46. Griffiths, P.; van der Linden, S.; Kuemmerle, T.; Hostert, P. Pixel-Based Landsat Compositing Algorithm for Large Area Land Cover Mapping. *IEEE J. Sel. Top. Appl. Earth Obs. Remote Sens.* **2013**, *6*, 2088–2101. [CrossRef]
47. Karan, S.K.; Samadder, S.R.; Maiti, S.K. Assessment of the capability of remote sensing and GIS techniques for monitoring reclamation success in coal mine degraded lands. *J. Environ. Manag.* **2016**, *182*, 272–283. [CrossRef]
48. Feng, Y.; Wang, J.; Bai, Z.; Reading, L. Effects of surface coal mining and land reclamation on soil properties: A review. *Earth Sci. Rev.* **2019**, *191*, 12–25. [CrossRef]
49. Lima, A.T.; Mitchell, K.; O'Connell, D.W.; Verhoeven, J.; Van Cappellen, P. The legacy of surface mining: Remediation, restoration, reclamation and rehabilitation. *Environ. Sci. Policy* **2016**, *66*, 227–233. [CrossRef]
50. Kennedy, R.E.; Yang, Z.Q.; Gorelick, N.; Braaten, J.; Cavalcante, L.; Cohen, W.B.; Healey, S. Implementation of the LandTrendr Algorithm on Google Earth Engine. *Remote Sens.* **2018**, *10*, 691. [CrossRef]
51. Dai, G.S.; Ulgiati, S.; Zhang, Y.S.; Yu, B.H.; Kang, M.Y.; Jin, Y.; Dong, X.B.; Zhang, X.S. The false promises of coal exploitation: How mining affects herdsmen well-being in the grassland ecosystems of Inner Mongolia. *Energy Policy* **2014**, *67*, 146–153. [CrossRef]
52. Wu, Z.; Lei, S.; Lu, Q.; Bian, Z.; Ge, S. Spatial distribution of the impact of surface mining on the landscape ecological health of semi-arid grasslands. *Ecol. Indic.* **2020**, *111*, 105996. [CrossRef]
53. Li, J.; Deng, X.J.; Yang, Z.; Liu, Q.L.; Wang, Y.; Cui, L.Y. A Method of Extracting Mining Disturbance in Arid Grassland Based on Time Series Multispectral Images. *Spectrosc. Spectr. Anal.* **2019**, *39*, 3788–3793.
54. Xu, J.; Zhao, H.; Yin, P.; Jia, D.; Li, G. Remote sensing classification method of vegetation dynamics based on time series Landsat image: A case of opencast mining area in China. *EURASIP J. Image Video Process.* **2018**, *1*, 113. [CrossRef]
55. Dlamini, L.Z.D.; Xulu, S. Monitoring Mining Disturbance and Restoration over RBM Site in South Africa Using LandTrendr Algorithm and Landsat Data. *Sustainability* **2019**, *11*, 6916. [CrossRef]
56. Li, C.; Li, H.; Li, J.; Lei, Y.; Li, C.; Manevski, K.; Shen, Y. Using NDVI percentiles to monitor real-time crop growth. *Comput. Electron. Agric.* **2019**, *162*, 357–363. [CrossRef]
57. Fang, C.; Wen, Z.; Li, L.; Du, J.; Liu, G.; Wang, X.; Song, K. Agricultural Development and Implication for Wetlands Sustainability: A Case from Baoqing County, Northeast China. *Chin. Geogr. Sci.* **2019**, *29*, 231–244. [CrossRef]
58. Aqiang, Y.; Chuang, L.; Jianrong, F.; Jinling, Z.; Jing, T. The Application of High Spatial Resolution Remote Sensing Image forVegetation Type Recognition in Dagou Valley. In *Geoinformatics 2008 and Joint Conference on GIS and Built Environment: Classification of Remote Sensing Images*; International Society for Optics and Photonics: Bellingham, WA, USA, 2008; Volume 7147.
59. Pericak, A.A.; Thomas, C.J.; Kroodsma, D.A.; Wasson, M.F.; Ross, M.R.V.; Clinton, N.E.; Campagna, D.J.; Franklin, Y.; Bernhardt, E.S.; Amos, J.F. Mapping the yearly extent of surface coal mining in Central Appalachia using Landsat and Google Earth Engine. *PLoS ONE* **2018**, *13*, e0197758. [CrossRef]
60. Lei, S.; Bian, Z.; Daniels, J.L.; He, X. Spatio-temporal variation of vegetation in an arid and vulnerable coal mining region. *Min. Sci. Technol. (China)* **2010**, *20*, 485–490. [CrossRef]